Steady-state properties of the wideband semiconductor optical amplifier

K. ALFARAMAWI*, O. MAHRAN, W. EL SHIRBEENY S. ABBOUDY
Physics Department, Faculty of Science, Alexandria University, Alexandria, Egypt.

The gain characteristics for a bulk InP-InGaAsP homogeneous buried ridge stripe semiconductor optical amplifier are investigated. A wideband steady-state model is applicable. The gain spectrum is calculated at three different temperatures (*T*) of 220, 260 and 300 K and active region carrier concentrations (*n*) of 2.5 x 10^{24}, 2.6 x 10^{24}, 2.7 x 10^{24} m^{-3}. It is found that the peak of the gain increases by increasing the active region carrier density at constant temperature and amplifier length. In contrast, the gain is lowered by increasing the temperature at fixed carrier density and cavity length. The effect of the amplifier length on the system characteristics is also studied. The longer the amplifier the higher the gain at constant *T* and *n*. The influence of the injected current on the fiber to fiber gain is investigated for different temperatures. A gain saturation is noticed at temperatures below 220 K for current exceeding 80 mA.

(Received September 21, 2007; accepted October 31, 2007)

Keywords: Semiconductor optical amplifier, Signal gain coefficient, Carrier concentration

1. Introduction

Semiconductor optical amplifiers (SOA) are of great interest in all optical network systems because of their simultaneous fast switching and signal amplification capabilities [1]. The gain and noise figure are important characteristics of the semiconductor optical amplifiers, which are essential for the future of optical information systems and in wavelength division multiplexing (WDM) systems. Overall transmission capacity depends significantly on the spectral characteristics of the optical amplifiers, such as flatness, bandwidth, and the magnitude of the gain. [2].

In a semiconductor optical amplifier or laser amplifier, it is possible to assume a uniform carrier distribution along the cavity length *(z* direction) and consequently to neglect the variation of material gain with z. This approximation allows a simple description of the evolution with time of carriers and photons with rate equations independent of z [3]. This case is usually referred to steady state at which the variation of the carrier concentration is considered to be a constant along the amplifier cavity.

In this paper, we studied the effect of the change of a set of parameters on the gain of a bulk InP–InGaAsP homogeneous buried ridge stripe semiconductor optical amplifier. These parameters are the concentration of the carriers, the temperature, the length of the SOA and the injected current.

2. Theoretical model

2. 1. The material gain coefficient

The SOA modeled is a 1.55 μm InP–In_{1-x} Ga_x As_y P_{1-y} homogeneous buried ridge stripe device [4]. *x* and *y* are the molar fractions of gallium and arsenic, respectively, in the undoped active region. Lattice matching is assumed, for which $x = 0.47\ y$ [4]. The InGaAsP direct band-gap bulk-material active region has a material gain coefficient g_m (m^{-1}) given by [5],

$$g_m(\nu,n)=\frac{c^2}{4\sqrt{2}\pi^{3/2}n_1^2\tau\nu^2}\left(\frac{2m_e m_{hh}}{\hbar(m_e+m_{hh})}\right)^{3/2}\times\int_0^{\infty}\left[\sqrt{\nu'-\frac{E_g(n)}{h}}(f_c(\nu')-f_v(\nu'))\times\left(\frac{2T_0}{(1+(2\pi T_0)^2(\nu'-\nu)^2}\right)\right]d\nu' \quad (1)$$

where the symbol mean:

c	speed of light in a vacuum
υ	Optical frequency
n_1	active region refractive index
τ	radiative carrier recombination lifetime
$\hbar$	Planck's constant h divided by 2π;
m_e, m_{hh}	conduction band (CB) electron and valence band (VB) heavy hole effective masses, respectively;
n	CB carrier (electron) concentration.
T_0	mean lifetime for coherent interaction of electrons with a monochromatic field and is of the order of 1 ps.

The model is based on the assumption that there is a finite probability that a state in the conduction band will be occupied by an electron and/or a state in the valence band will be empty (of electron). If we denote an energy in the valence band by E_b and an energy in the conduction band by E_a , the values of each are given by [5]

$$E_a=(h\upsilon-E_g(n))\frac{m_{hh}}{m_e+m_{hh}} \quad (2)$$

$$E_b = -(h\upsilon - E_g(n))\frac{m_e}{m_e + m_{hh}} \tag{3}$$

The band-gap energy $E_g(n)$ can be expressed as

$$E_g(n) = E_{g0} - \Delta E_g(n) \tag{4}$$

E_{g0}, the bandgap energy with no injected carriers, is given by the quadratic approximation [6]

$$E_{g0} = e(a + by + cy^2) \tag{5}$$

where *a, b* and *c* are the quadratic coefficients and *e* the electronic charge. $\Delta E_g(n)$ is the bandgap shrinkage due to the injected carrier density. An expression for the band gap shrinkage, originally derived by Wolff [7], is given by

$$\Delta E_g(n) = eK_g n^{1/3} \tag{6}$$

where K_g is the bandgap shrinkage coefficient. The probabilities of the conduction band state f_c and valence band state f_v are given by Fermi-Dirac distributions [5]. In equation (1), it is possible to make the substitution

$$\left(\frac{2T_0}{(1+(2\pi T_0)^2(\nu'-\nu)^2)}\right) = \delta(\nu - \nu') \tag{7}$$

Hence, equation (1) becomes

$$g_m(\nu, n) = \frac{c^2}{4\sqrt{2}\pi^{3/2} n_1^2 \tau \nu^2}\left(\frac{2m_e m_{hh}}{\hbar(m_e + m_{hh})}\right)^{3/2} \times \sqrt{\nu - \frac{E_g(n)}{h}}(f_c(\nu) - f_v(\nu)) \tag{8}$$

g_m is composed of two components, a gain coefficient g'_m (≥0) and an absorption coefficient g''_m (≥0), so

$$g_m = g'_m - g''_m \tag{9}$$

where

$$g'_m = \frac{c^2}{4\sqrt{2}\pi^{3/2} n_1^2 \tau \nu^2}\left(\frac{2m_e m_{hh}}{\hbar(m_e + m_{hh})}\right)^{3/2} \sqrt{\nu - \frac{E_g(n)}{h}}\ f_c(\nu)(1 - f_v(\nu)) \tag{10}$$

$$g''_m = \frac{c^2}{4\sqrt{2}\pi^{3/2} n_1^2 \tau \nu^2}\left(\frac{2m_e m_{hh}}{\hbar(m_e + m_{hh})}\right)^{3/2} \sqrt{\nu - \frac{E_g(n)}{h}}\ f_v(\nu)(1 - f_c(\nu)) \tag{11}$$

2. 2 Gain of SOA

The gain *G*(dB) of the amplifier is given as [5]

$$G(\nu) = \frac{(1-R_1)(1-R_2)G_s}{(1-\sqrt{R_1R_2}G_s)^2 + 4G_s\sqrt{R_1R_2}\sin^2(\phi)} \tag{12}$$

where R_1 and R_2 are the input and output facet reflectivity respectively, and ϕ is the single pass shift. Our approximation based on the assumption that the amplifier is too short so that no Amplified Spontaneous Emission (ASE) is considered. On the other hand steady state case is proposed. Therefore one could put ϕ equals zero in equation (20) and then the amplifier gain is given by

$$G(\nu) = \frac{(1-R_1)(1-R_2)G_s}{(1-\sqrt{R_1R_2}G_s)^2 + 4G_s\sqrt{R_1R_2}} \tag{13}$$

G_s, the single-pass gain at optical frequency ν is given by [9]

$$G_s(\nu) = \exp\{\int_0^L [\Gamma g_m(\nu, n) - \alpha(n)]\, dz\}. \tag{14}$$

The material loss coefficient α (m^{-1}) is modeled as a linear function of carrier density [10]

$$\alpha(n) = K_o + \Gamma K_1 n \tag{15}$$

K_o and K_1 are the carrier-independent and carrier-dependent absorption loss coefficients, respectively. Γ is the optical confinement factor of the SOA.

3. Simulation method

The SOA model equations cannot be solved analytically, so a numerical solution is required. The material gain coefficient equations are solved first using equations (2-11) and this is implemented in a computer program with the aid of equations (14) and (15) to calculate the gain spectrum. The calculations are performed periodically by changing temperatures, carrier concentrations and SOA lengths each time. Finally the gain dependence of the injected current is computed by another program in which a set of equations including the threshold current and the characteristic currents are fed. The numerical values used in the simulations are given in table (1).

Table. 1. The numerical values used in the simulations.

Symbol	Parameter	Value
y	Molar fraction of Arsenide in the active region	0.892
Γ	Optical confinement factor	0.45
K_g	Bandgap shrinkage coefficient	0.9×10^{-10} eVm
n_1	InGaAsP active region refractive index	3.22
n_2	InP region refractive index	3.167
R_1	Input facet reflectivity	5.0×10^{-5}
R_2	Output facet reflectivity	5.0×10^{-5}
K_o	Carrier independent absorption loss coefficient	6200 m^{-1}
K_1	Carrier dependent absorption loss coefficient	7500 m^2
a	Bandgap energy quadratic coefficient	1.35
b	Bandgap energy quadratic coefficient	-0.775
c	Bandgap energy quadratic coefficient	0.149
m_e	Effective mass of electron in the CB	4.10×10^{-32} kg
m_{hh}	Effective mass of a heavy hole in the VB	4.19×10^{-31} kg
m_{hl}	Effective mass of a light hole in the VB	5.06×10^{-32} kg

4. Results and disscusion

Fig. 1 shows the signal gain and stimulated gain coefficients g_m and g_m', respectively, as a function of signal wavelength in the range of 1300 to 1650 nm.

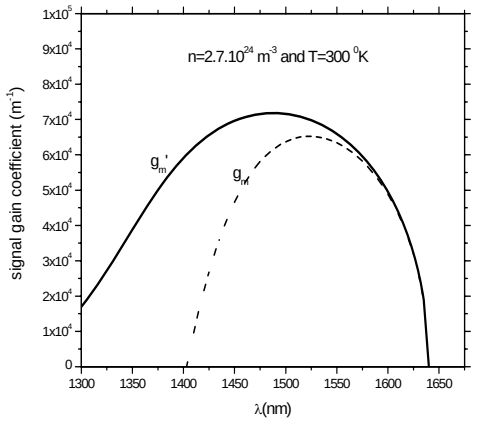

Fig. 1. The variation of signal gain and stimulated emission gain coefficients with wavelength at room temperature (300 K)

The calculations were performed at room temperature (300 K) and carrier concentration of the active material of 2.7×10^{24} m^{-3}. The value of the maximum gain coefficient (6.4×10^4 m^{-1}) was observed among the wavelength 1525 nm. In order to examine the factors affecting the gain coefficient, variation of the signal gain coefficient was studied at different temperatures and carrier concentrations.

Fig. 2 demonstrates the change of the signal gain (g_m) and absorbed gain (g_m'') coefficients spectra at temperatures 220, 260 and 300 K and carrier concentration 2.7×10^{24} m^{-3}. It is clear that by increasing the temperature, the lower-cut off of g_m shifts up towards the longer wavelength while the maximum value of g_m decreases. On the other hand, g_m'' decreases exponentially with wavelength, and for a proper range of wavelength (1325-1500 nm) its value increases with temperature.The depression of the maximum gain with increasing the temperature might be attributed to the fact that the carrier-carrier scattering at high T leads to an increase in the absorption rate and this, consequently, leads to an obvious decrease in the signal gain.

Furthermore, both g_m and g_m'' are estimated among the desired wavelength range at different carrier concentration of the bulk SOA system. The temperature was maintained at 300 K. Figure 3 represents g_m and g_m'' spectra at three carrier concentrations, namely 2.5×10^{24}, 2.6×10^{24} and 2.7×10^{24} m^{-3}.

The general behavior of g_m spectrum is the same as that discussed above. In contrast to the trend with T, the lower-cut off of g_m shifts towards the shorter wavelength with increasing the carrier density, while its peak value increases with n at constant temperature. This is probably due to stimulation effects as the carrier concentrations are injected.

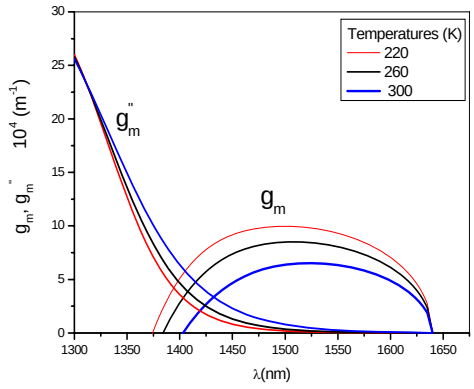

Fig. 2. Signall gain and absorption gain coefficients against wavelength calculated at three properly- selected temperatures.

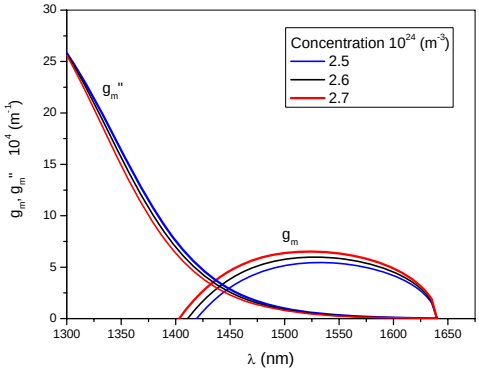

Fig. 3. Signal gain and absorption gain coefficients against wavelength calculated at three different carrier concentrations.

The amplifier gain (G) spectrum at different temperatures is depicted in Figure 4. The calculations are proceeded at carrier density of 2.7 x 10^{24} m^{-3} and amplifier length of 100 μm.

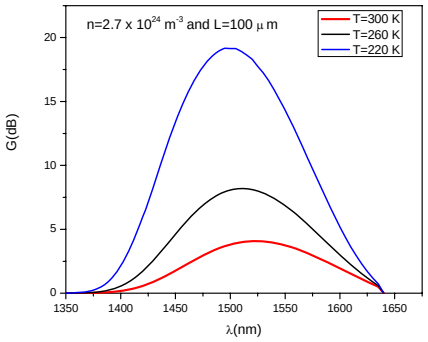

Fig. 4. Amplifier gain against wavelengths at amplifier length of 100 μm and 2.7× 10^{24} m^{-3} concentration.

It is well obvious that the peak value of the gain increases largely when the temperature is lowered from room temperature down to 220 K. Even longer gain peak could be obtained at lower temperatures. As the amplifier gain and the gain coefficient are intercorrelated, a similar trend with T is then expected.

A close inspection of Fig. 4 reveals that the peak value of the gain is shifted towards lower wavelengths by lowering T. If we denote the value of the wavelength corresponding to the maximum gain by λ_{center} one can conclude a relationship between λ_{center} and T at constant n and L. Fig. 5 illustrates this relationship. It is clear that a linear relationship of the form $\lambda_{center} = AT + B$ can be obtained in the studied temperature range, where A and B are the fitting parameters.

The dependence of G on the medium carrier density is shown in Figure 6. The peak value of G increases monotonically by increasing the concentration of the carriers. This trend is very similar to that of the gain coefficient as the carrier density is changed, see Fig. 3.

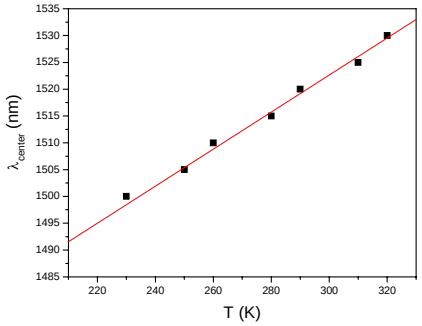

Fig. 5. Relationship between the temperature and the wavelength at maximum gain.

The influence of the amplifier length on the gain is also studied for the selected range of wavelengths. In figure 7 the gain is plotted against wavelength at different amplifier lengths. While the gain peak increases by increasing the amplifier length, the broadening of the curve becomes worth at higher L which is not favored in semiconductor optical amplifier WDM systems. Hence it is recommended for the communication systems to choose the amplifier in the range of 100 μm.

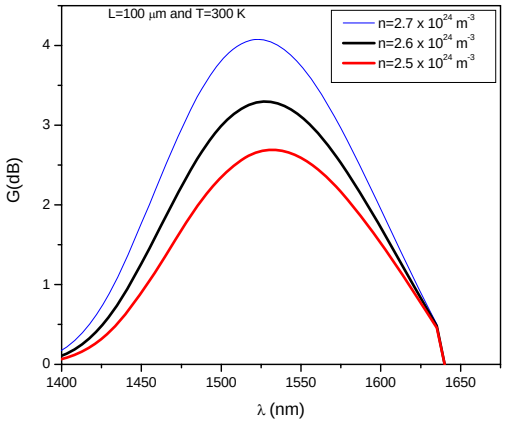

Fig. 6. Gain against wavelength at room temperature for different concentrations.

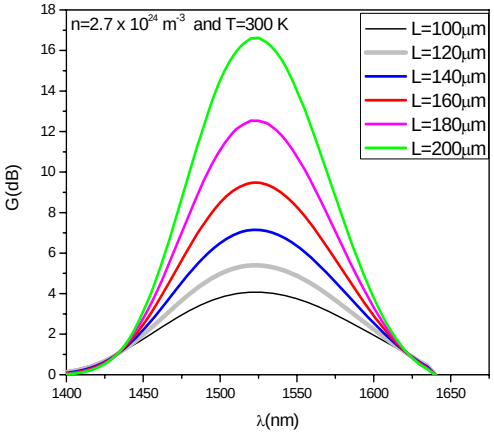

Fig. 7. Amplifier gain against wavelength at different amplifier lengths at room temperature and selected concentration.

Fig. 8 introduces the effect of the injected current on the fiber-to-fiber gain at different temperatures. It is noticed that saturation occurs at all values of temperatures and for currents above ~ 70 mA.

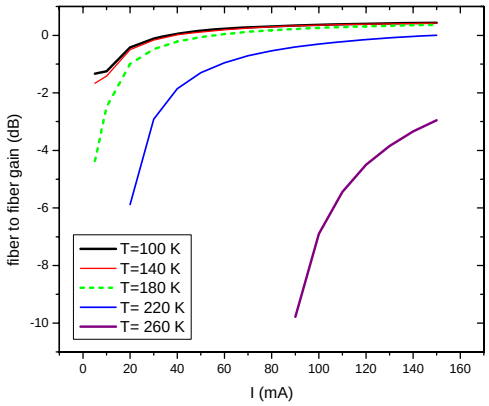

Fig. 8 Fiber-to-fiber gain against the injected current at different temperatures.

5. Conclusions

The gain spectra of InP-InGaAsP semiconductor optical amplifier system are studied. The calculations are performed at different temperatures, active medium carrier density and amplifier length. The peak of the amplifier gain increases by lowering the temperature. The wavelength corresponding to the maximum gain is found to be linearly dependent on T. Increasing the carrier density leads to an increase in the peak of the amplifier gain and this is explained as probably due to stimulation effects at high *n*. The gain peak is elevated as the amplifier length is increased but the curve becomes narrower, which is not recommended for WDM systems.

References

[1] T. Numai, IEEE J. of Quantum Electron. **28**, 1513 (1992).
[2] L. Goldberg, D. Mehuys, M. R. Surette D. C. Hall, J. Quantum Electron. **29**, 2028 (1993).
[3] Philippe Brosson, J. Lightwave Technology, **12**(l), 49 (1994).
[4] Michael J. Connelly, IEEE J**.** of Quantum Electron., **37**, 439 (2001).
[5] Michael J. Connelly, Semiconductor optical amplifiers, Boston-London 2002.
[6] S. Adachi, Physical Properties of III–IV Semiconductor Compounds.New York: Wiley, 1992.
[7] P. A. Wolff, Phys. Rev. **126**, 405 (1962).
[8] N. G. Nilsson, Appl. Phys. Lett., **33**, 653 (1978).
[9] D. A. Marcuse, IEEE J. Quantum Electron., QE-**19**, 63 (1983).
[10] Y. Suematsu, A. R. Adams, Handbook of Semiconductor Lasers and Photonic Integrated Circuits, London, U.K., Chapman & Hall, 1994.

*Corresponding author: kalfaramawi@yahoo.com